

22 **Abstract**

23 The purpose of this study was to develop micron-sized droplet emulsions able to increase the heat
24 deposition of high intensity focused ultrasound (HIFU), aiming to accelerate the tumour ablation in
25 highly perfused organs with reduced side effects. The investigated droplets consisted of a
26 perfluorooctyl bromide (PFOB) core coated with a biocompatible fluorinated surfactant called F-TAC.
27 The novelty of this work relies on the use, for this application, of a high boiling point perfluorocarbon
28 core (142°C), combined with an in-house fluorinated surfactant to formulate the emulsion, yielding
29 quasi-reversible strong interactions between the HIFU beam and the droplets. In order to fine-tune
30 the emulsion size, surfactants with different hydrophobic/hydrophilic ratios were screened. Different
31 concentrations of PFOB droplets were homogeneously embedded in two different MRI compatible
32 tissue mimicking materials (TMM), exhibiting either ultrasound (US) absorbing or non-absorbing
33 properties. For the US absorbing TMM, the speed of sound at each droplet concentration was also
34 assessed. These TMM were sonicated by 1 MHz HIFU with acoustical power of 94 W at two different
35 duty cycles. The temperature elevation was monitored accurately by MRI proton shift resonance
36 frequency in near real-time. The presence of sono-sensitive droplets induced a significant increase of
37 the HIFU thermal effect that persisted under repeated sonication of the same locus. Optimal
38 enhancement was observed at the lowest concentration tested (0.1%) with an additional
39 temperature rise at the focal point of approximately 4 °C per applied kJ of acoustic energy
40 corresponding to one order of magnitude augmentation of the thermal dose. Furthermore, no
41 deformation of the heating pattern pre- or post-focal was observed.

42

43 1. Introduction

44

45 High intensity focused ultrasound (HIFU) is a promising non-invasive and non-ionizing
46 treatment for ablation of solid tumours.^{1,2} It has FDA approval for the treatment of uterine
47 fibrosis³, and is in clinical development to treat several solid malignant tumours including
48 liver, prostate, breast, bladder, kidney and soft tissue sarcoma.⁴⁻¹⁰ However, it possesses
49 several shortcomings such as long treatment duration to fully ablate the tumour^{1,11} and, for
50 deep-seated tumours, high ultrasound (US) intensity is required leading to an increase in
51 side effects. In addition, even when US energy is concentrated to the focal point, it can also
52 be deposited along the US beam in front or behind the focus point and cause severe side
53 effects such as skin and bone burning.^{8,12-14} Furthermore, given a treatment planning, inter-
54 patient variation in the volume and shape of the lesion may be difficult to control and to
55 reproduce.¹⁵

56 The ablative effects of HIFU are due to the focusing of high energy beams in a small
57 region on the order of the wavelength, *i.e.* on the millimetre scale.¹ At the focal spot, the
58 temperature can rise by 15 to 50 °C within seconds, resulting in a rapid blood coagulation
59 and inducing cell necrosis. The damage to the tumours involves two synergistic phenomena.
60 The first is the thermal deposition of energy and is proportional to the coefficient of
61 absorption of the tissue. The second is the inertial cavitation (IC)¹ yielding mechanical
62 damages to cell structure and that can also increase the thermal effect consecutive to the
63 emission of acoustic waves at higher frequency than the incident beam, that is, mode
64 conversion phenomenon.¹⁶

65 Several approaches have been investigated to amplify the thermal delivery during
66 HIFU and hence to decrease the occurrence of side effects. The first approach was to use
67 microbubbles (MB) filled with perfluorocarbon (PFC) gas that were originally used for
68 ultrasound contrast enhancement.^{11,17,18} The MB serve as nuclei for inertial cavitation (IC)
69 and act as enhancers of tissue heating rate as they absorb energy from the sound wave
70 when they oscillate.^{16,19} However, as they are ultra-sensitive to US with a very low IC
71 pressure threshold, they may cause unwanted damage along the US beam due to
72 vaporisation of bubbles and/or initiation of IC, producing unwanted side effects such as
73 uncontrollable pre-focal lesion and skin burn.^{11,19} Additionally, they exhibit a limited

74 circulation half-life as gases diffuse rapidly in tissue. To overcome this limitation, an
75 alternative approach would be to produce bubbles *in-situ* without an exogenous agent,
76 however this method it is not satisfactory because of the high IC threshold of tissues, and
77 the results can be highly variable due to the natural heterogeneity of tissues.²⁰

78 The use of acoustic droplet vaporisation (ADV) was suggested to be more
79 advantageous to the same purpose. The concept of ADV consists of using phase shift
80 droplets (PSD) filled with a liquid PFC that undergoes a phase change from liquid to gas
81 under the induction of an US wave.^{21,22} PFC droplets are able to vaporise, like any volatile
82 liquid, provided a sufficient decrease in pressure below their vapour pressure or an increase
83 in temperature above their boiling point. Under HIFU conditions, at the focal point, the
84 negative pressure peak is sufficient to vaporise droplets into bubbles with a volumetric
85 expansion at least 5 to 6 times the parent droplets. The resulting bubbles can be
86 spatiotemporally controlled^{23,24} and, conversely to their unexcited liquid counterpart,
87 possess better echogenic properties. The acoustic negative peak pressure necessary for this
88 vaporisation depends on several factors, such the nature of PFC core, the type of shell and
89 droplet size. These exogeneous droplets that provide bubbles *in-situ* act as nuclei for *in vivo*
90 cavitation leading to tissue heating and lesion.^{25,26} Moreover, the formation of a bubble
91 cloud would mostly reflect the incident ultrasonic beam and thus protect the far field tissues
92 from US wave effect.^{27,28} The backward reflected wave would also contribute to an increase
93 in the pressure amplitude in front of the bubble cloud and hence help further vaporisation.²²

94 Like microbubbles, droplets are usually constituted of two parts: the core which
95 contains at least one type of PFC and the shell made of a pure surfactant or a mixture of
96 surfactants. For a given droplet composition, the size is an important feature for its
97 vaporisation threshold, as a consequence of the Laplace pressure inside the droplet which is
98 inversely proportional to its radius and to the interfacial pressure between the two liquids.
99 Therefore, ADV requires more energy than the theoretical condition when a droplet was in
100 contact with air. The larger the droplet, the lower the energy required to vaporise it.^{24,29} The
101 choice of PFC core is a key factor. Several groups^{30,31} have developed superheated PFC filled
102 droplets, which consist of a PFC with low boiling temperature, usually below human body
103 temperature, that remains in liquid state at 37 °C thanks to either the Laplace pressure and
104 interfacial tension or the metastability of the superheated liquid PFC against homogeneous
105 nucleation.³²

106 This allows a decrease in the energetic vaporisation threshold and even the use of
107 diagnostic US apparatus for this purpose. Droplets have another major advantage as they
108 possess a longer circulation half-life than their gaseous homologues.²²

109 There are two kinds of PSD. The first are PFC nanodroplets constituting
110 nanoemulsions, called phase shift nanoemulsions (PSNE). Taking advantage of the enhanced
111 permeability retention (EPR) effect, they can extravasate from the neovasculature and
112 accumulate in the tumour microenvironment. These PSNE are used for imaging and/or
113 therapy.³³⁻³⁵ The second are micron-sized droplets (MSD) which are restrained to the
114 vasculature (endo-vascular). They can be used for enhancing thermal ablation in highly
115 perfused tumours^{15,36} and as well for embolotherapy as they generate micro-bubbles able to
116 occlude small capillary vessels.^{23,37}

117 In order to reduce the potential side effects ascribed to HIFU therapy when adapting
118 it to highly perfused tumours, we report the use of perfluorooctylbromide (PFOB)-filled MSD
119 to reduce the ultrasound exposure time and energy required for tumour ablation.
120 Conversely to other reported studies, we used a PFC with a high boiling point (142 °C) in
121 order to gain in droplet stability²⁶ and allowing a reverse phase shift once the HIFU beam is
122 stopped, in order to avoid cellular and tissue damage as well as blood vessel occlusion.²¹ In
123 other terms, high boiling point PFC droplets undergo quasi-reversible interactions with the
124 HIFU beam, which subsequently avoids possible capillary occlusion due to volume
125 expansion, permits recirculation of droplets in the blood stream after exposure to the HIFU
126 and enables accurate spatial control of the thermal effects localized around the focal point.
127 PFOB, a FDA approved PFC was used as a potential blood substitute because of its oxygen
128 high solubilising ability, inertness and stability.^{38,39} It was shown that a formulation of PFOB
129 with lecithin possesses a very low toxicity with a LD₅₀ in rats of 45 g/kg and a short half-life in
130 the body of about 4 days for 2.5 g/kg administrated.⁴⁰

131 PFC droplets need to be stabilised with amphiphilic molecules such as lipids or
132 fluorinated surfactants.⁴¹ The present study uses in-house surfactants called F-TAC which
133 consist of a fluorinated hydrophobic moiety exhibiting a high affinity for PFC droplets and a
134 hydrophilic moiety made of a polyTRIS oligomer⁴² (See Figure 1a). Contrary to commercially
135 available fluorinated surfactants often used in the literature, such as ZONYL (Dupont De
136 Nemours) and CAPSTONE (Chemours), F-TAC surfactants exhibit a good biocompatibility (no

137 hemolytic activity, LD₅₀ up to 4.5g/kg in rats after *i.v.* administration), have a ubiquitous
138 distribution in rat after *i.v.* or *per os* route, and display a long half-life (30-50h) without any
139 degradation in both plasma and tissues.^{43,44}

140
141 The main goal of the study is the enhancement of HIFU mediated heat deposition by
142 MSD embedded in tissue mimicking material. The influence of the F-TAC chemical structure
143 modification on droplet size and the impact of MSD concentration on the enhancement of
144 HIFU thermal effect was assessed. To do so, the droplets were embedded either in an
145 acoustically absorbent agar-based TMM that mimics the acoustic properties of soft tissue,⁴⁵
146 or in a non-absorbent material made of gelatine gel to gain a better understanding of the
147 mechanism of action of MSD. The velocity of sound in the used gel was assessed, as that gel
148 preparation underwent some substantive change to be compatible with magnetic resonance
149 (MR) imaging and guidance of the HIFU sonication. Given that the depth of US penetration is
150 inversely proportional to the frequency, a 1 MHz frequency used for HIFU sonification was
151 considered to be a good compromise for deep tissue application, for instance in the liver or
152 kidney. The temperature rise was monitored accurately throughout the gel by proton
153 resonance shift frequency (PRSF) MR thermometry, and a diagnostic ultrasound device was
154 used to investigate the attenuation of the backscattered signal from MSD doped gels.

155 2. Experimental (material and methods)

156 2.1. Material

157 Agar, SiO₂ (1.5 and 0.5 μm), Al₂O₃ (3 and 0.3 μm) were purchased from AlfaAeser (Karlsruhe,
158 Germany), glycerol from Acros and Benzalkonium chloride (BAL) from Sigma-Aldrich (St.
159 Quentin Fallavier, France), PFOB from Fluorochem (Hadfield, United Kingdom), 1H,1H,2H,2H-
160 perfluorooctanethiol was graciously provided by Atomchem (Colombes, France), and all
161 other reagents (sodium trifluoroacetate, AIBN) and solvents were of reagent grade.

162

163 2.2. Surfactant synthesis

164 In order to fine-tune the MSD size and to understand the surfactant chemical structure vs
165 droplet size relationship, several in-house surfactants called F-TAC were screened. F-TAC are
166 constituted of a non-ionic polar head comprising of n repeating
167 Tris(hydroxymethyl)aminomethane (TAC_n) units (n=DP_n is the average degree of
168 polymerization) and of a hydrophobic perfluorinated tail (F₆=C₆F₁₃C₂H₄ or F₈=C₈F₁₇C₂H₄) (See
169 Figure 1a).

170 Due to the fluorine-fluorine interaction, the fluorinated part of these amphiphilic molecules
171 exhibits a high affinity for the perfluorocarbon core of the droplets while their polar head
172 ensures the whole water solubility.⁴³ Their synthesis previously described by Pucci et al.⁴⁶
173 was easily performed in one step by free radical polymerisation, allowing a swift supply of
174 surfactant of high quantity. For a given perfluorocarbon core, the size of the resulting MSD is
175 on one hand correlated to the concentration and chemical structure of the surfactant and,
176 on the other hand, to the level of energy delivered to the solution during the emulsification
177 process.^{42,47} The chemical composition of the liquid core, the surfactant concentration and
178 the process conditions were kept constant and only the impact of the surfactant chemical
179 structure was assessed. Two different series were studied, each one being characterised by
180 the length of its hydrophobic tail. The first one is the F₆ series with F₆=C₆F₁₃C₂H₄, while the
181 second one is the F₈ series with F₈=C₈F₁₇C₂H₄. Three different polar head sizes were tested
182 for each series, with a respective DP_n of 7, 12, 29 for the first series and 7, 13, 18 for the
183 second series.

184 All surfactants were easily synthesised by free radical polymerisation in one step
185 using two different perfluoroalkanethiols C₆F₁₃C₂H₄SH or C₈F₁₇C₂H₄SH as transfer reagents
186 (telogen) and azobisisobutyronitrile (AIBN) as a radical initiator. Ten ml of solvent were used

187 per gram of tris(hydroxymethyl) acrylamidomethane (THAM) ($C = 0.57 \text{ mol/L}$) and the
188 concentration of AIBN was 0.5 eq of telogen. R_0 is the telogen/monomer molar ratio. The
189 summary of the different polymerisation conditions is listed in Table 1.

190 Briefly, in a shlenck tube, dry methanol or a mixture of methanol and water (9/1) for
191 the highest DPn, AIBN, THAM and telogen agent were added, the mixture underwent three
192 cycles of freeze, vacuum, thaw and then was heated at 90°C for 4 hours under vigorous
193 stirring until complete disappearance of the monomer. Then the crude product was
194 precipitated twice in diethyl ether and filtrated and dried to recover the expected compound
195 as a white powder with yields ranging from 31.8% to 84.0% (see Table 1). The DPn was
196 assessed by ^{19}F -NMR as described previously.⁴²

197

198 2.3. MSD preparation

199 For our therapeutic purpose, the maximum droplet size in terms of vascular circulation is 6
200 μm , given the strong requirement to avoid capillary blockage and to allow them to be
201 transpulmonary.²¹ In preliminary studies (data no shown) we noticed that employing a high
202 energy process using an ultrasonic device (Bioblock Scientific Vibracell 75043, 13-mm
203 diameter sonotrode) always led to a bimodal population, one in a the nanometric range and
204 one in the micrometric range. Accordingly, the emulsion was prepared using a low energy
205 process using a homogeniser as with a Polytron® system PT 3100 homogenizer from
206 Kinematica (Luzern Switzerland). General procedure: To prepare a 10% volume fraction
207 emulsion, 835 mg of surfactant were dissolved in 58.5 ml of water then 6.5 ml of PFOB were
208 added. The resulting mixture was cooled down with an ice bath and then the resulting
209 emulsion was homogenised three times 15 min at 22500 rpm. Finally, the emulsion was kept
210 at 4°C until use.

211

212 2.4. Gel preparation

213 As a proof of concept for the enhancement of HIFU-induced heat deposition by MSD and
214 accurate MR thermometry, MSD were embedded into a tissue mimicking material (TMM).
215 There are numerous TMM available, among them the most common are agar, urethane
216 rubber, zerdine, silicone polyvinyl alcohol, polyacrylamide and gelatine.⁴⁸⁻⁵⁰ We decided to
217 use the well characterised agar-based gel as it possesses several advantages such as having a
218 sound velocity value close to that of soft tissue, it exhibits almost a linear response of

219 attenuation to frequency and it can be stored for several weeks.⁴⁵ Furthermore, this TMM
220 possesses a high melting point of about 80°C and is reusable compared to other gels such as
221 BSA-loaded polyacrylamide.⁵¹

222

223 *2.4.1. Agar gel (sample #1 and #2)*

224 The composition of the TMM gel⁴⁵ was modified in order to be compatible with our
225 experimental setting. The main components of the gel are water, glycerol and agar, the first
226 two compounds mainly contribute to the sound velocity value, while the last one contributes
227 to the stiffness of the gel. The Al₂O₃ powder, which delivers the attenuation properties of
228 the gel, had to be substituted with SiO₂ because of its interaction with the magnetic field
229 resulting in low MRI signal especially with T₂* sequences as for PRFS thermometry. The
230 incorporation of SiC, which mimics the backscattering properties along with Al₂O₃, was also
231 suppressed as it was not mandatory for our purpose.

232 **General procedure:** Proportions of the different ingredients other than water used to reach
233 a constant 290 ml of final gel are provided in mass unit (gram): glycerol = 33.6, BAL = 0.27,
234 agar = 9, SiO₂ (1.5µm) = 2.85, SiO₂ (1.5µm) = 2.64. Silicon oxide was suspended in 50 ml of
235 degassed water and insonified with a 13 mm sonotrode for 2 min in. The BAL solution,
236 glycerol, the silicon oxide mixture and degassed water (see Table 2) were added to a 400 ml
237 tared beaker. And under mechanical stirring the mixture was heated and then agar was
238 added. The solution was heated at above 90°C for one hour. Then the gel was set to cool
239 down under magnetic stirring and any water lost was compensated with degassed water.
240 Then when the mixture reached about 40°C; the emulsion (see Table 2), loaded with three
241 drops of methylene blue, was added, homogenised and cool down. The volume fraction of
242 PFOB in TMM was used to describe the MSD concentration (see Table 2).

243 *2.4.2. Gelatine gel (sample #3 and #4)*

244 The purpose of this section was to identify the dominant mechanism producing enhanced
245 acoustic absorption among two hypotheses: 1) the MSD are directly converting the
246 mechanical energy into thermal energy; 2) the MSD act as inelastic scatters producing mode
247 conversion and re-emitting higher frequency than the incident one, with the higher
248 frequencies being absorbed more effectively by the surrounding bulk gel.⁵² If the second
249 hypothesis is true, the efficiency of micro-particles should be significantly decreased in a

250 non-absorbent gel. If the first hypothesis is true, their efficiency should be comparable when
251 embedded in an absorbent or non-absorbent bulk gel.

252 A non-acoustic absorbent gel was prepared with water, gelatine and benzalkonium
253 chloride and its acoustic properties were measured. 9 g of gelatine (brand Vahiné), 285 mg
254 of BAL were added to 276 ml of degassed water. Then the mixture was heated at 45°C for 5-
255 10 min to ensure complete dissolution of the gelatine. The mixture was left to cool down to
256 25°C and poured in an open glass cylinder, with its base closed by paraffin film. Then 15 ml
257 of emulsion was added and then cooled drawn at 4°C. For the control gel, we used the same
258 protocol, but 285 ml of degassed water was added.

259

260 2.5. Physical characterization

261

262 2.5.1. Particle size

263 The particle size distribution was assessed using a *Mastersizer 2000* laser diffraction *particle*
264 *size* analyser (Malvern Instruments, Orsay, France) equipped with Hydro2000S as sample
265 dispersion unit (A) mod using the Mie light scattering theory. The refractive indices used
266 were 1.305 for the PFOB and 1.333 for the dispersant (water). Several drops of the emulsion
267 were added with a stirring of 500 rpm to the sample dispersion unit. The Mie theory was
268 used to determine the volume weighted mean diameter $D[4,3]$ and the polydispersity was
269 calculated as d_{90}/d_{10} . d_{90} is the diameter at which 90% of the sample's volume is
270 comprised of droplets with a diameter less than this value. d_{10} is the diameter at which 10%
271 of the sample's volume is comprised of droplets with a diameter less than this value. The size
272 distribution histogram is shown in Figure 1b.

273

274 2.5.2. Optical microscopy

275 The optical microscopy was performed on an Olympus BX60 microscope (Olympus, Rungis,
276 France) with 100x magnification (see Figure 1c) and no spectral filter.

277

278 2.5.3. Determination of volume fraction

279 All spectra were recorded on a 400 MHz Bruker Avance II spectrometer with a resonance
280 frequency of 376.53 MHz for ^{19}F . ^{19}F -NMR spectra were acquired using the inverse-gated

281 decoupling technique. Each spectrum was the result of 256 scans with 131 072 data points
282 using a relaxation delay of 4 s. Peak area was integrated using manufacturer standard
283 software (Topspin, version 3.5pl7, Bruker, Wissembourg, France). A calibration curve was
284 obtained using a mixture of 40 μl of PFOB dissolved in 2.9004 g (4.068 ml) of Et_2O and a
285 dilution path produced various concentrations. Twenty μl of water were diluted with 600 μl
286 of MeOH, then 600 μl of various concentration Et_2O /PFOB mixture were added. For the
287 titration, the volume of water was replaced by 20 μl of emulsion and 600 μl Et_2O were added
288 instead of the mixture Et_2O /PFOB. Et_2O was used to solubilise the PFOB and MeOH to have
289 a homogeneous solution. The mixture was homogenised, then 500 μl of this solution were
290 added to the NMR tube, followed by a coaxial capillary filled with a solution of sodium
291 trifluoroacetate (TFA) salt in D_2O (50mg/ml). The latter was used as external reference and
292 was kept the same for all experiments. The TFA salt was chosen because of the proximity of
293 the signal ascribed to its CF_3 group compared to the CF_3 of the PFOB, at -75.96 and 80.15
294 ppm respectively, thus avoiding problem of keeping a uniform field over a long range. The
295 ratio of integration of the external standard over that of PFOB was plotted against the
296 volume fraction of PFOB to create a calibration curve. All measurements were performed on
297 triplicate samples.

298

299 *2.5.4. Acoustic velocity measurement*

300 Measurement of sound velocity was performed using the setup schematically described in
301 SI. During a measurement, a burst made of one sinusoidal period was generated by a wave
302 function generator (model 33250A from Agilent, les ulis, France). The burst intensity was
303 amplified 500 times using a RF power amplifier (model A 10-100 from M2S, Argelès sur Mer,
304 France), then went through a duplexer (model RDX-6 from RITEC, Warwick, USA) and
305 eventually reached a transducer. We used three transducers (from Panasonics, Gennevilliers,
306 France) that differ by their resonance frequency; 2.25, 5 and 10 MHz. The burst sinusoidal
307 frequency was chosen to match the transducer central frequency. The transducer was in
308 contact with a gel immersed in water. The short pressure wave produced by the transducer
309 propagated through the gel until it reached the opposed edge of the gel that is in contact
310 with a metallic surface. The wave was reflected back to the transducer and converted into an
311 electrical signal that was sent by the duplexer to a pre-amplifier (PAS-0.1-20 from RITEC),
312 then to a Broadband receiver (BR-640A from RITEC). The signal was visualised on an

313 oscilloscope (model WaveSurfer 424 from Lecroy, Courtaboeuf, France) and recorded after
314 averaging over 400 sweeps. The same measurement was performed after removing the gel
315 where the signal propagates over exactly the same distance in water. The squared signal
316 amplitude was analysed. The temporal position of reflected pulses (determined from its
317 center of gravity) was simply a multiple n times the time 2τ to travel forward and back
318 through the gel. The corresponding forward and back travelling distance, that is twice the gel
319 thickness δ , was determined from the signal measured after removing the gel and using the
320 known ultrasound velocity of water (that is 1480 m/s at a temperature of 20°C). The sound
321 velocity in the gel was then calculated as an average value of sound velocities derived from τ
322 and δ for the n reflected pulses.

323

324 2.6. Thermo-acoustic investigation of TMM gels doped with MSD

325

326 2.6.1. *Focused ultrasound*

327 A spherical MR-compatible phased array HIFU transducer (Imasonic, Besançon, France)
328 composed of 256 elements was used for generation of focused ultrasound. The main
329 parameters are frequency range 974 - 1049 kHz, focal length 130 mm and aperture 140 mm.
330 The transducer was supplied by a 256-channel beam former (Image Guided Therapy, Pessac,
331 France). The HIFU transducer was placed horizontally on the MR table and emitted vertically.
332 Each gel sample (agarose-based and gelatine-based) was placed in an ultrasound coupling
333 holder filled with degassed water and maintained with a standardised setup using resin
334 moulds (Figure 2 a,b). A standard ultrasonic gel was added on the sample top to avoid
335 interface reflection of the waves. The standardised setup assured reproducible positioning of
336 the sample and a 35 mm identical depth of the focus through the series of experiments.
337 HIFU sonication was performed using the electronic steering of the beam thus describing
338 iteratively a discrete circular pattern of 4 mm diameter composed of 16 points regularly
339 distributed on the circumference. This sonication pattern was chosen in order to average
340 eventual local inhomogeneities of the TMM gel or MSD distribution in the gel, which could
341 exist at infra-millimeter scale. The pattern was covered in 1.65 s and the trajectory was
342 repeated 20 times, yielding a total treatment time of 33 s. The applied acoustic power was
343 94W and the beam emission duty cycle was set at 70% (sample #1 absorbent gel and #3 non-
344 absorbent ge) or 90% (sample #2 absorbent and #4 non-absorbent). This is respectively

345 equivalent to 1.4 s or 1.8s cumulated sonication time per ietration locus, corresponding to
346 an effective duty cycle of sonication of droplets (as seen at a given location in the gel) of
347 4.2% and 5.5%. Sonication planning and hardware control was achieved using
348 Thermoguide™ software (Image Guided Therapy, Bordeaux, France).

349 The mechanical effect of HIFU sonication on the MSD size distribution was
350 investigated in a liquid emulsion using a fixed focal point beam, applied power 135 W, pulse
351 duration 90 ms, duty cycle 90 %, total duration of the sonication paradigm 33 s. To this
352 purpose 3ml of emulsions of MSD stabilized with F₆TAC₇ or F₈TAC₇ respectively were inserted
353 in an ultrasound-transparent container centered on the focal point and exposed one, two or
354 three times to the sonication paradigm, separated by 5 minutes intervals. The particle size
355 distribution was measured using the *Mastersizer 2000* laser diffraction *particle size* analyser
356 as described above.

357

358

359 2.6.2. MR thermometry

360 All measurements were performed using a 3T whole body MR system (Prisma Fit, Siemens,
361 Erlangen, Germany). An 11-cm diameter receive only loop coil was used and placed around
362 the sample. High resolution MR thermometry was performed by Proton Resonance
363 Frequency Shift (PRFS) thermometry,⁵³ which provides a precise monitoring of temperature
364 evolution at a high frame rate and with a millimetre resolution. To this purpose we used a
365 segmented GRE-EPI sequence with main parameters; TE (echo time) = 10ms, TR (repetition
366 time) = 25ms, flip angle = 8°, BW (bandwidth) = 550Hz/pixel, acquisition matrix 128×128,
367 slice thickness = 5mm, FOV = 128 x 128mm, voxel size = 1x1x5mm³, temporal resolution = 1
368 s., number of averages NSA (number of averages) = 1, phase encoding direction = head-foot
369 (HF), spectroscopic fat saturation.

370 The MSD effect of enhancing the HIFU absorption was measured with two
371 normalized metrics: 1) a differential heating factor was defined as the additional elevation of
372 temperature at the focal point considered at the end point of the sonication interval divided
373 by the total emitted acoustic energy of the sonication [unit °C/kJ], and 2) an integral
374 enhancement of heating was defined as the thermal energy deposited in the MR slice
375 integrated over the voxels heated at least +1°C above baseline at the end point of the
376 sonication interval and divided by the total emitted acoustic energy of the sonication

377 [dimensionless]. The thermal energy was calculated as the product temperature elevation
378 times estimated heat capacity.

379 A total of 38 sonications were analyzed in absorbent or non-absorbent gels doped
380 with MSD and compared with 36 baseline sonications in MSD-free gels.

381

382 2.6.3. Treatment planning

383 Positioning of the focal point was prescribed using 3D high resolution images acquired with
384 an isotropic gradient echo sequence with the following parameters: TE = 2.46 ms, TR = 5.36
385 ms, flip angle = 10°, BW = 390 Hz/pixel, slices per slab = 192, FOV = 256 x 256 mm, slice
386 thickness = 0.8 mm, voxel size = 1.00 x 1.00 x 1.28mm. The focal plane was set at 35 mm
387 depth in the sample in the direction of propagation of the HIFU beam.

388

389 2.6.4. ¹⁹F MRI of MSD loaded TMM samples

390 ¹⁹F image acquisition of the samples was performed using an RF-spoiled 2D gradient-recalled
391 echo (GRE) pulse sequence in order to confirm the uniform distribution of micro-particles in
392 the gel. A dedicated ¹⁹F quadrature RF-birdcage coil was used, switchable between ¹H and
393 ¹⁹F (Clinical MR solutions, Brookfield, WI).⁵⁴ The resonance frequency for ¹⁹F was 115.95
394 MHz. The coil had internal diameter 4.4 cm and 6 cm length. Due to the small size of the
395 coil, subsamples were cut from the TMM gel native and doped with 0.1% and 0.5% MSD v/v
396 and stacked parallel inside the coil in a miniature water bath, which improved the local
397 magnetic field homogeneity (passive shimming). Main parameters of the gradient echo ¹⁹F
398 sequence were TR = 300 ms, TE = 5.07 ms, NSA = 25, BW = 325Hz/pixel, matrix 96 x 96, FOV
399 = 128 x 128mm, flip angle = 70°, slices per slab = 8, slice thickness = 10 mm, pulse duration =
400 2 ms, in plane voxel size = 1.67 x 1.33 mm².

401

402 2.6.5. Ultrasonography

403 The acquisition of ultrasound images to investigate the attenuation of the backscattered
404 signal from gel samples was performed using a clinical US system (ACUSON Antares, Siemens
405 Healthcare, Mountain View, CA). The abdominal imaging probe composed of 192 elements
406 operated in harmonic mode at 2.2 MHz. Appropriate near field coupling and far field full
407 absorption of the acoustic field was implemented to avoid beam reflections.

408 3. Results and discussion

409

410 3.1. Characterization of microdroplets

411 As shown in Table 3, for all surfactants, except for the F₈TAC₁₃ and F₈TAC₁₇, MSD possess a
412 size distribution in the micrometric range. For a given hydrophobic tail, the larger the polar
413 head, the smaller the resulting MSD size until reaching a plateau. For both series, the
414 optimal polar head size was found to be around 12 Tris units. Above this value of DP_n, the
415 MSD size remains constant for both hydrophobic tails. Furthermore, the size decreased by a
416 factor 6.5 between DP_n 7 and 13 for the F₈ series, while for the F₆ series the size decreases
417 only by a factor 2.5 between DP_n 7 and 12. On one hand, this trend can be explained by the
418 fact that, during the emulsification process, increasing the polar head size increases the
419 steric hindrance and hence the stability of the MSD until an optimal size is reached.⁴¹ On the
420 other hand, once this plateau is achieved (for DP_n ≥ 12), the hydrophobic tail seems to play a
421 significant role, as the MSD diameter obtained for F₈TAC₁₃ is twice smaller than for F₆TAC₁₂.
422 This might be either due to an optimal volume ratio between the polar head and the
423 hydrophobic tail of the surfactant and/or to a higher concentration of available surfactant (in
424 the form of free monomer or micelles) in the dispersant phase (*i.e.* water). In the case of
425 F₈TAC₁₃ this leads to a finer emulsion. The surfactant concentration is about 8 (for F₆TAC₁₂)
426 and 280 (for F₈TAC₁₃) times over the critical micellar concentration (CMC). It is noteworthy
427 that this difference in droplet size cannot be ascribed to a difference in surface tension
428 between PFOB and water in the presence of each surfactant as they are similar with 12.1 mN
429 m⁻¹ for F₆TAC₁₂ and 10.4 mN m⁻¹ for F₈TAC₁₃.⁴² Emulsions were stable for several weeks in the
430 refrigerator which is in good agreement with previous work from other groups.¹⁵ Our group
431 has previously shown that the surfactant type F₆TAC₇ is perfectly biocompatible after *i.v.*
432 injection in mice (LD50 above 4.5g/kg).⁴³

433 Given that droplets need to be smaller than 6 μm in diameter to avoid capillary
434 thrombosis, and that the larger the droplets diameter the lower the energy required for
435 their vaporisation,⁵⁵ MSD made with either F₈TAC₇ or F₆TAC₇ surfactant appear to be the
436 best candidates. For the first emulsion the d₉₀ is above 7 μm, while for the second emulsion,
437 d₉₀ was below 6 μm in diameter which makes the latter one a better candidate. However, as
438 shown by the MSD size distribution in Figure 1.b, the droplets obtained with F₆TAC₇

439 displayed a very high polydispersity ($d_{90}/d_{10}=4.00$)⁴² which was also confirmed by optical
440 microscopy (Figure 1.c).

441 The method of MSD titration was modified from the one published by Astafyeva et al⁴² in
442 order to obtain a totally homogenous solution containing both PFOB and water. To do so, we
443 used a ternary system made of a mixture of methanol and diethyl ether, the latter being
444 used to ensure complete solubilisation of PFOB in the solution.⁵⁶ The concentration of PFOB
445 in the emulsion was thus estimated to be 11.6 ± 0.9 %, which indicated a loss of about 15%
446 of water during the synthesis process.

447

448 3.2. MR compatibility and acoustics properties

449 The final gel composition demonstrated perfect MR compatibility in term of local magnetic
450 susceptibility and was shown to be homogeneous at the observation scale of the MR (mm-
451 range), as illustrated in Figure 2 a,b. High resolution GRE proton 3D images also
452 demonstrated that no macroscopic air bubbles were present.

453 The sound velocity of our TMM was found 1522 ± 5 m/s at 1 MHz, 1521 ± 5 m/s at
454 2.5 MHz, 1528 ± 5 m/s at 5 MHz and 1532 ± 5 m/s at 10 MHz. These values are close to the
455 speed of sound in soft tissue in vivo (approx. 1540 m/s). Furthermore, usually US devices are
456 calibrated at this speed of sound.⁵⁷ The speed of sound of our TMM is a little bit lower than
457 the one found in the original gel from Ramnarine et al.⁴⁵ Even if some TMM components
458 were changed, the sound velocity is only proportional to the quantity of water, agar and
459 glycerol and these were used in the same proportion as Ramnarine et al.⁵⁸ Furthermore,
460 approximately the same sound velocity is measured for the same TMM but without silica
461 (Data not shown). This discrepancy could be due to the use of different brand of agarose,
462 given that their mechanical properties change according to their molecular weight,⁵⁹ and
463 that change in molecular weight affects the gel elasticity with an elasticity decreasing
464 proportionally with the molecular weight.

$$465 \quad v = \sqrt{\frac{c_{ij}}{\rho}} \quad (1)$$

466 C_{ij} represents the stiffness coefficient, ρ the mass density and v the speed of sound.⁶⁰

467

468 3.3. Effect of MSD concentration on acoustic properties of the gel (echogenicity)

469 Four concentrations of MSD using F₆TAC₇ surfactant were embedded into the TMM to study
470 their impact on the acoustic and echogenic properties. The sound velocity in the different
471 TMM loaded with MSD decreased linearly as a function of their concentration, as PFOB
472 sound velocity is much lower, 623 m/s, than the control TMM, 1522 m/s.^{40,42}

473 The MSD were not hyper-echogenic in harmonic ultrasound images at 2.5 MHz (see
474 Figure 3) but increasing the MSD concentration induced a significant enhancement of the
475 attenuation of the backscattered acoustic signal as the far field signal become darker as the
476 concentration rises. The backscattered signal was plotted against the depth of the signal
477 source in the image, independently for the four different concentration TMM and fits to an
478 exponential decay function $f(x)=\exp(-a*x)$ with the linear attenuation coefficient “a”
479 decreasing linearly with droplets concentration.

480

481 3.4. MSD interaction with HIFU beam

482 3.4.1. *In absorbent TMM*

483 The ¹⁹F-MR imaging confirmed that the droplets were evenly distributed throughout the gel
484 on the scale of the current resolution (Figure 4).

485 Only the two lowest MSD concentrations were tested for HIFU thermal
486 enhancement, 0.1 and 0.5 % v/v. These concentrations are more realistic when considering
487 the feasible delivery in living tissue. The additional temperature elevation was approximately
488 9°C and 15°C for 0.1% and 0.5% concentration of MSD respectively, as illustrated in Figure 2
489 d-f and Figure 5a, which corresponds to an impressive thermal dose amplification by a factor
490 on the order of 2⁹ and 2¹⁵ respectively, according to Sapareto.⁶¹

491 Table 4 shows the results for the two defined metrics of HIFU enhancing effect in two series
492 of TMM samples, the precision of measurements, the values of the two tailed p-test and the
493 confidence interval (CI). As the p-value was always inferior to 10⁻⁵ in each comparative
494 branch, the reported number of replicates is clearly sufficient and allowed an estimation of
495 the enhanced heating efficacy with 6% precision (second metric). This value is considered
496 sufficient for *in vivo* application, given the other potential sources of errors in a biological
497 system that largely overweight this uncertainty.

498 The additional temperature elevation per unit of emitted acoustic energy (first
499 metric) was found 4.30 ± 0.39 °C/kJ in gel series #1 with 0.1% concentration of MSD, 3.45 ±
500 0.22°C/kJ in gel series #2 with 0.1% concentration of MSD, 7.32 ± 0.57 °C/kJ in gel series #1

501 with 0.5% concentration of MSD and 5.15 ± 0.28 °C/kJ in gel series #2 with 0.5%
502 concentration of MSD.

503 The application of the second metric of HIFU enhancing effect yielded an integral
504 enhancement of the thermal energy produced in the MR slice of $(3.56 \pm 0.44) \times 10^{-3}$ in the
505 gel series #1 with 0.1% concentration of MSD, $(4.03 \pm 0.32) \times 10^{-3}$ in the gel series #2 with
506 0.1% concentration of MSD $(6.51 \pm 0.72) \times 10^{-3}$ in the gel series #1 with 0.5%
507 concentration of MSD, and $(7.08 \pm 0.40) \times 10^{-3}$ in the gel series #2 with 0.5% concentration
508 of MSD. The precision and the confidence interval demonstrated relevant and reproducible
509 measurements.

510 The relationship between the MSD concentration and HIFU-induced heat generation
511 was not linear as demonstrated by the two metrics. This relationship was also observed with
512 PSNE where increasing the droplet concentration from 0.008 % to 0.020 % result in similar
513 lesion volume in a polyacrylamide gel.⁶²

514 Repeated acquisition of MR temperature maps in the plane parallel to the HIFU beam
515 propagation showed no evidence of pre- or post-focal thermal build up during the
516 volumetric HIFU exposure in presence of MSD (Figure 1.c). The heating patterns were
517 localised around the prescribed position of the focal plane and matched the near-elliptical
518 shape predicted by theory (*e.g.* non-distorted). These findings are very important in the
519 context of the lesion predictability. According to Chen et al,⁶³ the shape of the lesion was
520 demonstrated to change from a cigar shape to a teardrop shape in the presence of an
521 ultrasound contrast agent around 1 MHz frequency. Lo and Kripfgans⁶⁴ found similar results
522 by increasing the amplitude or the number of pulses. In our study, we have demonstrated
523 that the interaction between the HIFU beam and the home-made MSD did not result in the
524 distortion of the lesion shape, within the range of applied power and duty cycle of
525 sonication. This discrepancy might be explained by a different mechanism of interaction of
526 MSD with the acoustic waves. PFC possess a high ability to dissolve gas, especially oxygen,
527 and were reported in literature as oxygen carriers.³⁹ As postulated by Rapoport et al,³⁴
528 during the peak rarefactional pressure, the dissolved gas forms a bubble inside the MSD
529 shell, whereas the PFOB stay in liquid form. These bubbles are capable of undergoing stable
530 cavitation but are less prone to IC which might explain the difference of behaviour compared
531 to other study.²⁶

532

533

534 *3.4.2. Impact of acoustics gel properties on HIFU thermal enhancement by MSD*
535 *droplets*

536 HIFU sonication yielded a low temperature elevation of only 1.2°C in average in the non-
537 absorbent gel samples. Comparing the results of heating enhancement by 0.5% MSD in
538 absorbent and non-absorbent gel according to Tables 4 and 5 for the second metric and the
539 surfactant F₆TAC₇ show that the enhancement of the HIFU thermal effect was mainly due to
540 the presence of MSD (90% of the effect) and the intrinsic acoustical absorption properties of
541 the TMM had only a slight impact. The first metric was not used for this comparison as it
542 may be biased by the different heat diffusion coefficient of the gel matrix.

543

544 *3.4.3. Effect of choice of surfactant on the MSD ultrasound absorption*

545 The best potential candidate surfactant according to Table 3 regarding the average diameter
546 (F₈TAC₇ and F₆TAC₇) were investigated for comparative MSD effect on the HIFU absorption in
547 non-absorbent gel (Table 5, metric 2). The other surfactants were excluded because of the
548 small size of corresponding MSD. The integral enhancement of the thermal energy
549 deposition in the slice, comparing the 0% and 0.5% concentration of MSD was 6.1×10^{-3} in
550 non-absorbent gel using F₆TAC₇ and 4.4×10^{-3} in non-absorbent gel using F₈TAC₇ surfactant.
551 These MSD have comparable ultrasound absorption, but the choice of the surfactant is
552 important for an optimal effect of enhanced HIFU thermal therapy.

553

554

555 *3.4.4. Effect of repeated HIFU sonications on MSD*

556 Table 6 showed that after the repetition of HIFU exposure in the non-absorbent gel at
557 the same location, a slight decrease of 5% of thermal deposition per cycle was observed
558 between the first shot and the second shot and 10 % between the first shot and the third
559 shot, this tendency is also illustrated with graphical plots in Figure 5.b. This behaviour
560 confirms that the interaction between the HIFU beam and MSD is mainly a reversible
561 process within the range of sonication parameters used in our study. The measurable loss of
562 heat deposition efficacy between each sonication was observed under static conditions (*i.e.*
563 no blood flow) and indicated that the MSD distribution and concentration are marginally

564 evolving, for instance some droplets can coalesce or some of the PFC can be dissolved.⁶⁵ One
565 advantage of the MSD stability against repeated HIFU sonication is the reduction of the risk
566 of embolism.²⁶ Another advantage is the possibility to use respiratory gated sonication, i.e.
567 delivering temporal fractions of energy periodically and synchronized to tissue motion⁶⁶ in
568 order to target the same tissue despite patient breathing.

569 The repeated exposure of MSD liquid emulsion to HIFU beams yielded a reduction of
570 the average diameter in the range 25% to 75%, depending on the nature of surfactant and
571 on the number of applied cycles of sonication, as shown in Table 7. This result supports the
572 safe use of described endovascular MSD *in vivo*, as their size decreased upon application of
573 HIFU, without a risk of capillary embolism. Due to the large pool of circulating MSD in the
574 blood, the local denaturation (eg size reduction) of some MSD is not expected to impact the
575 final efficacy as new MSD are continuously supplied to the treated area.

576

577 3.4.5. Perspectives

578

579 In this proof of concept study, we demonstrated significant enhancement of the HIFU
580 absorption in presence of tailored-made sono-sensitive MSD, however, a parametric study
581 was not performed to determine the influence of the acoustic intensity levels and duration
582 of sonication on the enhancement effect. These investigations are required in order to
583 optimize the HIFU pulse sequence to be applied to the respective MSD.

584 Future *in vivo* studies need to be performed to confirm the thermal enhancement
585 produced by the current MSD. As compared to the present *in vitro* study, there are some
586 different conditions to be considered. Firstly, the fraction of acoustic power transferred to
587 tissue will change as the absorption properties, stiffness and viscosity will be different from
588 our TMM. Secondly, the droplets will be confined to the blood vessels as we target tumours
589 in highly perfused organs (*e.g.* kidney or liver). Thirdly, we may be not able to reach, *in vivo*,
590 the droplet concentration added to the gels, however, significant dose reduction is likely to
591 be achieved. According to Figure 5a, the 0.1% MSD gel was heated approximately 2.5 times
592 more than the baseline gel. This ratio largely exceeds the therapeutic need. One should also
593 note in this study that we used not more than 135 acoustic watt. Literature reports^{67,68}
594 mention significantly larger acoustic powers *in vivo* (ie between 300W and 800W).

595 Unlike phase shift nanoemulsions,³⁰ when using our micro-droplets, the sonication can
596 start a few minutes after the iv injection, as there is no need to wait some accumulation
597 period. Overall, a HIFU treatment session comprises 10 to 30 minutes of active sonication
598 interval and the MSD are required to be stable during a relatively short period of time.
599 The reported experiments were performed at ambient temperature to avoid a time-
600 consuming procedure of stabilizing the TMM temperature at 37 °C inside the MR bore. The
601 temperature can also influence the energy required for ADV and/or IC, knowing that ADV
602 depends both on thermal and acoustic parameters and the latter will foster the physical
603 interaction of HIFU beam with MSD.⁶⁵ The pool of MSD interacting with the HIFU beam will
604 be continuously refreshed *in vivo* due to the blood flow, supporting a higher efficiency.
605 Overall, the final efficacy *in vivo* remains to be determined.

606

607

608 **4. Conclusion**

609 As a proof of concept, MSD with a PFOB core were synthesised and introduced into a MRI
610 compatible TMM, in order to enhance the thermal deposition of focused ultrasound. We
611 expect that this effect will allow a decrease in the energy and the time required to perform
612 tumour ablation, and to reduce the risks of HIFU treatment side effects by decreasing the
613 thermal build up in the near and far field.

614 By varying the chemical structure of an in-house fluorinated surfactant, the size of
615 the MSD could be tuned in the range 0.67 to 4.07 μm . These droplets were embedded in a
616 common agar-based TMM, which mimics the acoustic properties of soft tissue. The gel
617 composition was modified to be MR compatible by substituting the Al_2O_3 by SiO_2 and the
618 acoustic properties of this TMM new formulation were assessed, yielding a sound velocity
619 very similar to soft tissue.

620 TMM loaded with various concentrations of MSD did effectively enhanced the
621 heating efficiency around the focal point, potentially reducing treatment time for a given
622 target level of temperature. We noticed that the thermal deposition was not linear with
623 MSD concentration in TMM gels, and that the best specific activity was obtained *in vitro* at
624 0.1% concentration. Furthermore, the reiteration of the HIFU burst at the same location only
625 lessened by about 5 % the efficacy of heat deposition between each repetition in static
626 conditions (non-circulating droplets). Moreover, the acoustic properties of the material had

627 little if any influence on the efficiency of the MSD, translated into similar enhancement in
628 both absorbent and non-absorbent gel. Further investigations are required to assess the
629 exact mechanism of acoustic energy conversion into thermal energy, specifically if the
630 droplets undergo phase transition or not. Future studies are planned using *ex vivo* perfused
631 kidney in order to prove that this effect is transposable to highly perfused organs.
632

634 **References**

- 635 1 J. Kennedy, *Nat. Rev. Cancer*, 2005, **5**, 321–327.
- 636 2 C. Moonen, B. Quesson, R. Salomir, F. Vimeux, J. de Zwart, J. van Vaals, N. Grenier and
637 J. Palussière, *Neuroimaging Clin. N. Am.*, 2001, **11**, 737–47, xi.
- 638 3 D. Tyshlek, J.-F. Aubry, G. ter Haar, A. Hananel, J. Foley, M. Eames, N. Kassell and H. H.
639 Simonin, *J. Ther. Ultrasound*, 2014, **2**, 2.
- 640 4 O. Al-Bataineh, J. Jenne and P. Huber, *Cancer Treat. Rev.*, 2012, **38**, 346–353.
- 641 5 J.-F. Aubry, K. B. Pauly, C. Moonen, G. ter Haar, M. Ries, R. Salomir, S. Sokka, K. M.
642 Sekins, Y. Shapira, F. Ye, H. Huff-Simonin, M. Eames, A. Hananel, N. Kassell, A. Napoli,
643 J. H. Hwang, F. Wu, L. Zhang, A. Melzer, Y. Kim and W. M. Gedroyc, *J. Ther.*
644 *Ultrasound*, 2013, **1**, 13.
- 645 6 J. Kennedy, F. Wu, G. ter Haar, F. Gleeson, R. Phillips, M. Middleton and D. Cranston,
646 *Ultrasonics*, 2004, **42**, 931–935.
- 647 7 L. G. Merckel, L. W. Bartels, M. O. Köhler, H. J. G. D. van den Bongard, R. Deckers, W.
648 P. T. M. Mali, C. A. Binkert, C. T. Moonen, K. G. A. Gilhuijs and M. A. A. J. van den
649 Bosch, *Cardiovasc. Intervent. Radiol.*, 2013, **36**, 292–301.
- 650 8 J. Vidal-Jove, E. Perich and M. Alvarez del Castillo, *Ultrason. Sonochem.*, 2015, **27**, 703–
651 706.
- 652 9 F. Wu, Z. Wang, Y. Cao, W. Chen, J. Bai, J. Zou and H. Zhu, *Br. J. Cancer.*, 2003, **89**,
653 2227–2233.
- 654 10 Y.-F. Zhou, *World J. Clin. Oncol.*, 2011, **2**, 8–27.
- 655 11 Y.-S. Tung, H.-L. Liu, C.-C. Wu, K.-C. Ju, W.-S. Chen and W.-L. Lin, *Ultrasound Med.*
656 *Biol*, 2006, **32**, 1103–1110.
- 657 12 S. E. Jung, S. H. Cho, J. H. Jang and J.-Y. Han, *Abdom. Imaging*, 2011, **36**, 185–195.
- 658 13 J.-J. Li, G.-L. Xu, M.-F. Gu, G.-Y. Luo, Z. Rong, P.-H. Wu and J.-C. Xia, *World J.*
659 *Gastroenterol.*, 2007, **13**, 2747–2751.
- 660 14 Y. Y. Seo, J. H. O, H. S. Sohn, E. K. Choi, I. D. Yoo, J. K. Oh, E. J. Han, S. E. Jung and S.
661 H. Kim, *Nucl. Med. Mol. Imaging*, 2011, **45**, 268–275.
- 662 15 M. Zhang, M. L. Fabiilli, K. J. Haworth, F. Padilla, S. D. Swanson, O. D. Kripfgans, P. L.
663 Carson and J. B. Fowlkes, *Acad. Radiol.*, 2011, **18**, 1123–1132.
- 664 16 C. C. Coussios, C. H. Farny, G. Ter Haar and R. A. Roy, *Int. J. Hyperthermia*, 2007, **23**,
665 105–120.
- 666 17 S. Umemura, K. Kawabata and K. Sasaki, *IEEE Trans. Ultrason. Ferroelectr. Freq.*
667 *Control*, 2005, **52**, 1690–1698.
- 668 18 T. Yu, G. Wang, K. Hu, P. Ma, J. Bai and Z. Wang, *Urological Research*, 2004, **32**, 14–19.
- 669 19 L. C. Moyer, K. F. Timbie, P. S. Sheeran, R. J. Price, G. W. Miller and P. A. Dayton, *J.*
670 *Ther. Ultrasound*, 2015, **3**, 7.
- 671 20 S. Sokka, R. King and K. Hynynen, *Phys. Med. Biol.*, 2003, **48**, 223–241.
- 672 21 O. D. Kripfgans, J. B. Fowlkes, D. L. Miller, O. P. Eldevik and P. L. Carson, *Ultrasound*
673 *Med. Biol.*, 2000, **26**, 1177–1189.
- 674 22 Y. Zhou, *J. Ther. Ultrasound.*, 2015, **3**, 20.
- 675 23 O. D. Kripfgans, C. M. Orifici, P. L. Carson, K. A. Ives, O. P. Eldevik and J. B. Fowlkes,
676 *IEEE Trans. Ultrason. Ferroelectr. Freq. Control*, 2005, **52**, 1101–1110
- 677 24 C.-Y. Lin and W. G. Pitt, *Biomed Res. Int.*, 2013, **2013**, 404361.
- 678 25 T. Giesecke and K. Hynynen, *Ultrasound Med. Biol.*, 2003, **29**, 1359–1365.
- 679 26 N. Rapoport, K. H. Nam, R. Gupta, Z. Gao, P. Mohan and A. Payne, *J. Control. Release*,
680 2011, **153**, 4–15.
- 681

682 27 A. H. Lo, O. D. Kripfgans, P. L. Carson, E. D. Rothman and J. B. Fowlkes, *IEEE Trans.*
683 *Ultrason. Ferroelectr. Freq. Control*, 2007, **54**, 933–946.

684 28 M. Viallon, L. Petrusca, V. Auboiroux, T. Goget, L. Baboi, C. D. Becker and R. Salomir,
685 *Ultrasound Med. Biol.*, 2013, **39**, 1580–1595.

686 29 K. C. Schad and K. Hynynen, *Phys. Med. Biol.*, 2010, **55**, 4933–4947.

687 30 J. A. Kopechek, E. Park, C.-S. Mei, N. J. McDannold and T. M. Porter, *J. Healthc. Eng.*,
688 2013, **4**, 109–126.

689 31 P. S. Sheeran, V. P. Wong, S. Luo, R. J. McFarland, W. D. Ross, S. Feingold, T. O.
690 Matsunaga and P. A. Dayton, *Ultrasound Med. Biol.*, 2011, **37**, 1518–1530.

691 32 P. A. Mountford, W. S. Smith and M. A. Borden, *Langmuir*, 2015, **31**, 10656–10663.

692 33 T. O. Matsunaga, P. S. Sheeran, S. Luo, J. E. Streeter, L. B. Mullin, B. Banerjee and P. A.
693 Dayton, *Theranostics*, 2012, **2**, 1185–1198.

694 34 N. Rapoport, *Wiley Interdiscip. Rev. Nanomed. Nanobiotechnol.*, 2012, **4**, 492–510.

695 35 P. Zhang and T. Porter, *Ultrasound Med. Biol.*, 2010, **36**, 1856–1866.

696 36 O. D. Kripfgans, M. Zhang, M. L. Fabiilli, P. L. Carson, F. Padilla, S. D. Swanson, C.
697 Mougnot, J. B. Fowlkes and C. Mougnot, *J. Acoust. Soc. Am.*, 2014, **135**, 537–544.

698 37 M. Zhang, M. L. Fabiilli, K. J. Haworth, J. B. Fowlkes, O. D. Kripfgans, W. W. Roberts,
699 K. A. Ives and P. L. Carson, *Ultrasound Med. Biol.*, 2010, **36**, 1691–1703.

700 38 C. I. Castro and J. C. Briceno, *Artif. Organs*, 2010, **34**, 622–634.

701 39 J. G. Riess and M. P. Krafft, *Biomaterials*, 1998, **19**, 1529–1539.

702 40 M. P. André, T. Nelson and R. Mattrey, *Invest. Radiol.*

703 41 T. F. Tadros, in *Emulsion Formation and Stability*, Wiley-VCH Verlag GmbH & Co.
704 KGaA, 2013, pp. 1–75.

705 42 K. Astafyeva, L. Somaglino, S. Desgranges, R. Berti, C. Patinote, D. Langevin, F.
706 Lazeyras, R. Salomir, A. Polidori, C. Contino-Pepin, W. Urbach and N. Taulier, *J. Mater.*
707 *Chem. B*, 2015, **3**, 2892–2907.

708 43 J. Maurizis, M. Azim, M. Rapp, B. Pucci, A. Pavia, J. Madelmont and A. Veyre,
709 *Xenobiotica*, 1994, **24**, 535–541..

710 44 L. Zarif, J. Riess, B. Pucci and A. Pavia, *Biomater. Artif. Cells. Immobilization Biotechnol.*,
711 1993, **21**, 597–608.

712 45 K. Ramnarine, T. Anderson and P. Hoskins, *Ultrasound Med. Biol.*, 2001, **27**, 245–250.

713 46 C. Contino-Pepin, J. Maurizis and B. Pucci, *Curr. Med. Chem. Anticancer Agents*, 2002, **2**,
714 645–665.

715 47 Y. Singh, J. G. Meher, K. Raval, F. A. Khan, M. Chaurasia, N. K. Jain and M. K.
716 Chourasia, *J. Control. Release*, 2017, **252**, 28–49.

717 48 J. Browne, K. Ramnarine, A. Watson and P. Hoskins, *Ultrasound Med. Biol.*, 2003, **29**,
718 1053–1060.

719 49 M. O. Culjat, D. Goldenberg, P. Tewari and R. S. Singh, *Ultrasound Med. Biol.*, 2010, **36**,
720 861–873.

721 50 K. Zell and J. I. Sperl and M. W. Vogel and R. Niessner and C. Haisch, *Phys. Med. Biol.*, 2007,
722 **52**, N475.

723 51 A. Dabbagh, B. J. J. Abdullah, C. Ramasindarum and N. H. Abu Kasim, *Ultrason.*
724 *Imaging*, 2014, **36**, 291–316.

725 52 S. A. Goss, L. A. Frizzell and F. Dunn, *Ultrasound Med. Biol.*, 1979, **5**, 181–186.

726 53 Y. Ishihara, A. Calderon, H. Watanabe, K. Okamoto, Y. Suzuki and K. Kuroda, *Magn*
727 *Reson Med.*, , DOI:10.1002/mrm.1910340606.

728 54 O. Lorton, J.-N. Hyacinthe, S. Desgranges, L. Gui, A. Klauser, Z. Celicanin, L. A. Crowe,
729 F. Lazeyras, E. Allémann, N. Taulier, C. Contino-Pépin and R. Salomir, *J. Magn. Reson.*,
730 2018, **295**, 27–37.

731 55 O. Kripfgans, M. Fabiilli, P. Carson and J. Fowlkes, *J. Acoust. Soc. Am.*, 2004, **116**, 272–
732 281.
733 56 P. Babiak, A. Němcová, L. Rulišek and P. Beier, *J. Fluor. Chem.*, 2008, **129**, 397–401.
734 57 E. L. Madsen, J. A. Zagzebski and T. Ghilardi-Netto, *Med. Phys.*, 1980, **7**, 43–50.
735 58 S. Inglis, K. Ramnarine, J. Plevris and W. McDicken, *Ultrasound Med. Biol.*, 2006, **32**,
736 249–259.
737 59 V. Normand, D. L. Lootens, E. Amici, K. P. Plucknett and P. Aymard, *Biomacromolecules*,
738 2000, **1**, 730–738.
739 60 P. Laugier and G. Haiat, *Introduction to the Physics of Ultrasound*, 2010.
740 61 S. A. Sapareto and W. C. Dewey, *Int. J. Radiat. Oncol. Biol. Phys.*, 1984, **10**, 787–800.
741 62 P. Zhang, J. A. Kopechek and T. M. Porter, *J. Ther. Ultrasound*, 2013, **1**, 2.
742 63 W.-S. Chen, C. Lafon, T. J. Matula, S. Vaezy and L. A. Crum, *Acoust. Res. Lett. Online*,
743 2003, **4**, 41–46.
744 64 A. H. Lo, O. D. Kripfgans, P. L. Carson and J. B. Fowlkes, *Ultrasound Med. Biol.*, 2006,
745 **32**, 95–106.
746 65 A. Ishijima, J. Tanaka, T. Azuma, K. Minamihata, S. Yamaguchi, E. Kobayashi, T.
747 Nagamune and I. Sakuma, *Ultrasonics*, 2016, **69**, 97–105.
748 66 V. Auboiroux, L. Petrusca, M. Viallon, A. Muller, S. Terraz, R. Breguet, X. Montet, C. D.
749 Becker and R. Salomir, *BioMed Res. Int.*, 2014, **2014**, 9.
750 67 B. Quesson, C. Laurent, G. Maclair, B. D. de Senneville, C. Mougenot, M. Ries, T.
751 Carteret, A. Rullier and C. T. W. Moonen, *NMR Biomed*, **24**, 145–153.
752 68 D. Elbes, Q. Denost, C. Laurent, H. Trillaud, A. Rullier and B. Quesson, *Ultrasound Med.*
753 *Biol.*, 2013, **39**, 1388–1397.
754
755
756
757
758
759
760
761
762
763
764
765
766
767
768
769
770
771
772
773
774
775
776
777
778
779
780

781
782
783
784
785
786
787
788
789
790
791
792
793
794
795
796
797
798
799
800
801
802
803
804
805
806
807
808
809
810
811
812
813
814
815
816
817
818
819
820
821

822 **Tables**

823

824

Surfactant	F ₈ TAC ₇	F ₈ TAC ₁₃	F ₈ TAC ₁₇	F ₆ TAC ₇	F ₆ TAC ₁₂	F ₆ TAC ₂₉
1/R ₀	4	8	12	4	12	20
Yield	65.2%	84.0%	65.1%	63.4%	81.3%	31.8%

825

Table 1. Polymerisation condition of different F-TAC

826

	Control	0.1%	0.5%	1%	2%
H ₂ O *	251.6	248.3	236.6	221.6	191.6
emulsion	0	3	15	30	60

827 **Table 2.** Volume of water and emulsion added in the

828 TMM gel series (in mL).

829

830

831

	Control	0.1%	0.5%	1%	2%
Volume of H ₂ O (mL)*	251.6	248.3	236.6	221.6	191.6
Volume of emulsion (mL)	0	3	15	30	60

832 *This volume includes the 50 ml and 5 ml of water added to SiO₂ and BAL respectively

833

Table 2. Volume of water and emulsion added in the TMM gel series (in mL).

834

Surfactant	F ₈ TAC ₇	F ₈ TAC ₁₃	F ₈ TAC ₁₇	F ₆ TAC ₇	F ₆ TAC ₁₂	F ₆ TAC ₂₉
Size in μm	4.07 \pm 0.12	0.62 \pm 0.02	0.62 \pm 0.09	3.67 \pm 0.17	1.48 \pm 0.22	1.47 \pm 0.09
PDI (d ₉₀ /d ₁₀)	4.84	3.97	3.18	4.00	2.90	2.00

835 **Table 3.** Droplet's size and polydispersity according the surfactant structure

836

837

Difference between 0% and 0.1% concentration									
	N	Metric 1 (°C/kJ)	Precision (°C/kJ)	P test	95% CI	Metric 2 (J/kJ)	Precision (J/kJ)	P test	95% CI
#1 F ₆ TAC ₇	4	4.30	0.39	p<10 ⁻⁵	3.53-5.07	3.56	0.44	p<10 ⁻⁵	2.68-4.45
#2 F ₆ TAC ₇	5	3.45	0.22	p<10 ⁻⁵	3.02-3.88	4.03	0.32	p<10 ⁻⁵	3.39-4.67
Difference between 0% and 0.5% concentration									
	N	Metric 1 (°C/kJ)	Precision (°C/kJ)	P test	95% CI	Metric 2 (J/kJ)	Precision (J/kJ)	P test	95% CI
#1 F ₆ TAC ₇	4	7.32	0.57	p<10 ⁻⁵	6.18-8.47	6.51	0.72	p<10 ⁻⁵	5.08-7.95
#2 F ₆ TAC ₇	4	5.15	0.28	p<10 ⁻⁵	4.60-5.70	7.08	0.40	p<10 ⁻⁵	6.27-7.88

839

840 **Table 4.** Differential heating factor calculated according to first metrics of MSD absorption effect and integral
841 enhancement of thermal energy absorption by the MSD (second metrics), between 0.0% and 0.1%, and
842 between 0.0% and 0.5% shown for absorbent TMM gel series (sample #1 and #2). N stands for the replicates of
843 sonications.

844

Difference between 0% and 0.5% concentration

		N	Metric 1 (°C/kJ)	Precision (°C/kJ)	P test	95% CI	Metric 2 (J/kJ)	Precision (J/kJ)	P test	95% CI
#3	F ₆ TAC ₇	7	4.49	0.21	p<10 ⁻⁵	4.07-4.91	6.20	0.27	p<10 ⁻⁵	5.67-6.73
#4	F ₆ TAC ₇	6	3.77	0.39	p<10 ⁻⁵	2.99-4.54	5.95	0.42	p<10 ⁻⁵	5.11-6.80
#3	F ₈ TAC ₇	4	2.95	0.08	p<10 ⁻⁵	2.79-3.10	3.93	0.14	p<10 ⁻⁵	3.65-4.20
#4	F ₈ TAC ₇	4	2.90	0.17	p<10 ⁻⁵	2.57-3.23	4.87	0.30	p<10 ⁻⁵	4.28-5.47

845 **Table 5.** Differential heating factor calculated according to first metrics of MSD absorption effect and integral
846 enhancement of thermal energy absorption by the MSD (second metrics), between 0.0% and 0.5% shown for
847 non-absorbent TMM gel series (sample #3 and #4). N stands for the replicates of sonications.
848

	Sonication 1 vs 2	Sonication 1 vs 3
#3 Locus A	0.2 %	5.2 %
#4 Locus A	5.0 %	12.6 %
#4 Locus B	9.8 %	12.3 %
Average	5.0 %	10.0 %

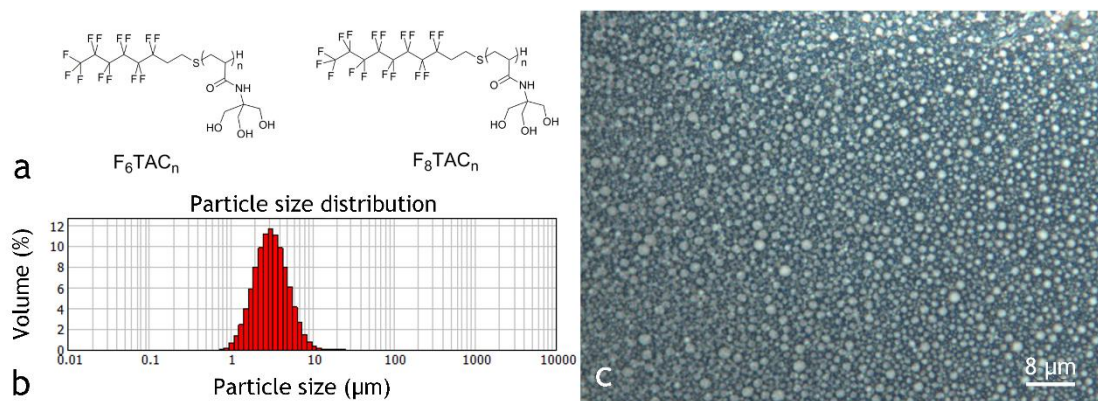
849 Attenuation of the differential integral enhancement of thermal energy (metric 2) between the first sonication
850 and the second sonication at the same location (first column) and between the first sonication and the third
851 sonication at the same location (second column), measured in non-absorbent gel #3 and #4.
852

HIFU cycles	F ₆ TAC ₇	F ₈ TAC ₇
0	4.963±0.465	5.634±0.273
1	3.132±0.066	1.434±0.014
2	2.021±0.546	1.242±0.020
3	1.693±0.016	1.364±0.110

853 **Table 7.** Effect of HIFU sonication on the MSD average size (units: μm), performed in a liquid emulsion, for two
854 surfactants. The sonication parameters per cycle pulse duration = 90 ms, duty cycle = 90 %, power = 135 W,
855 total duration 33s.
856
857
858
859
860
861
862
863
864
865
866
867
868
869
870

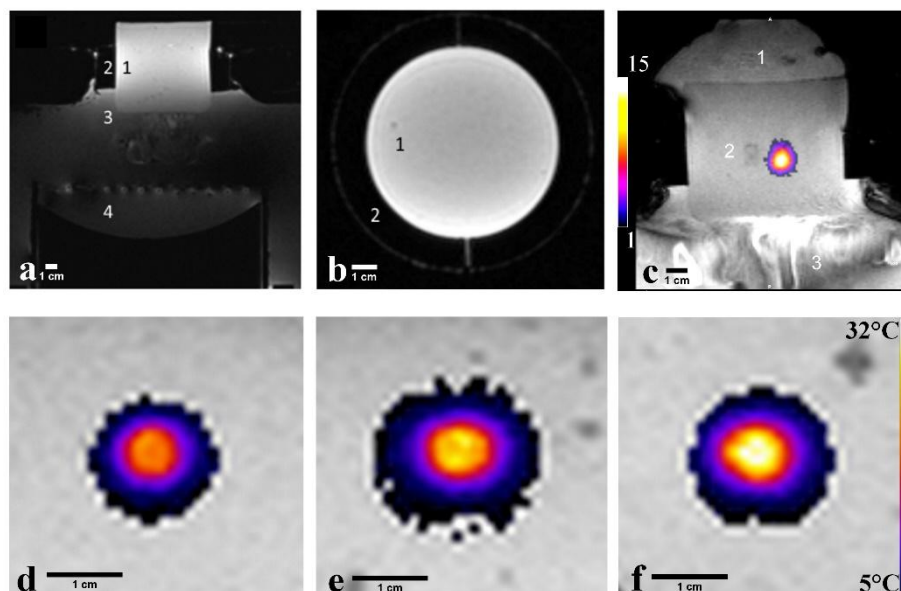
871
872
873
874
875
876
877

Figures



878
879
880
881
882
883
884

Figure 1 a) Chemical structure of fluorinated surfactant composed of two parts: a hydrophobic carbon chain bearing fluorine and hydrogen atoms ($C_6F_{13}C_2H_4$ or $C_8F_{17}C_2H_4$) and a hydrophilic part made of repeating TRIS units with an average number called DPn (for average degree of polymerisation), b) MSD particle size distribution in volume (Mastersizer 2000) made with F_6TAC_7 and c) Optical microscopy of MSD emulsion (x100) of concentration 10 % v/v



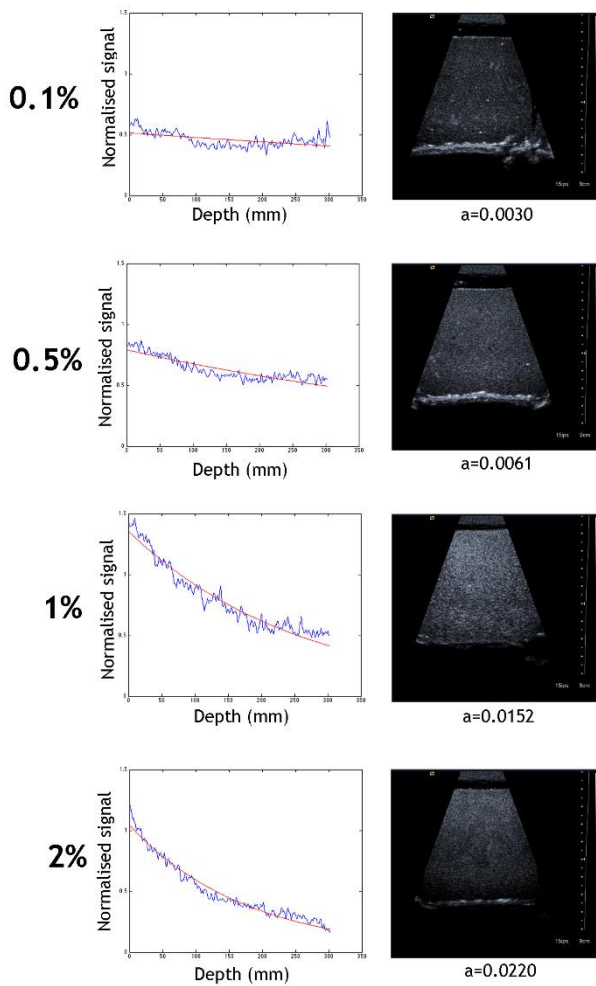
885
886
887
888

Figure 2. a,b) 3D MR images of the HIFU experimental set up: Transversal (a, FOV = 180 mm square) and Coronal (b, FOV = 120 mm square) planes; 1 Tissue mimicking gel, 2 Sample holder, 3 Degassed

889 water, 4 Concave surface of the HIFU applicator, c) Axial view of a magnitude MR image and PRF shift
 890 temperature elevation map overlay at the end point of a HIFU exposure in TMM gel loaded with 0.5%
 891 MSD concentration. Temperature elevation color map ranges from +1°C to +15°C. Shown FOV is 128
 892 mm square. Visible is the acoustic streaming in the coupling water layer (3), the TMM gel (2) and the
 893 standard ultrasonic gel on the top (1), assuring a non-reflective exit window distal. d,e,f) MR magnitude
 894 and overlaid PRF shift temperature elevation map at the end of HIFU exposure interval under identical
 895 sonication parameters in three TMM gels with (d) (e) (f); 0%, 0.1%, 0.5% MSD concentration
 896 respectively. Shown FOV is 30 mm.

897

898



899

900

901

902 **Figure 3.** Harmonic ultrasound imaging of loaded MSD gel at 2.2MHz for the four concentrations provided as
 903 embedded text. (Left) The fitted function of the backscattered signal corresponding to a decreasing
 904 exponential with the linear attenuation coefficient “a” expressed in units mm⁻¹. Experimental data was taken as
 905 the normalized average profile of the US signal intensity in a 150 pixel wide region of interest. (Right) The
 906 corresponding native US images.

907

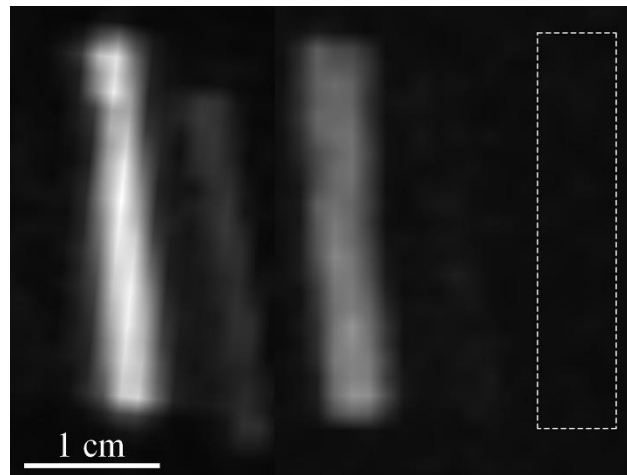
908

909

910

911

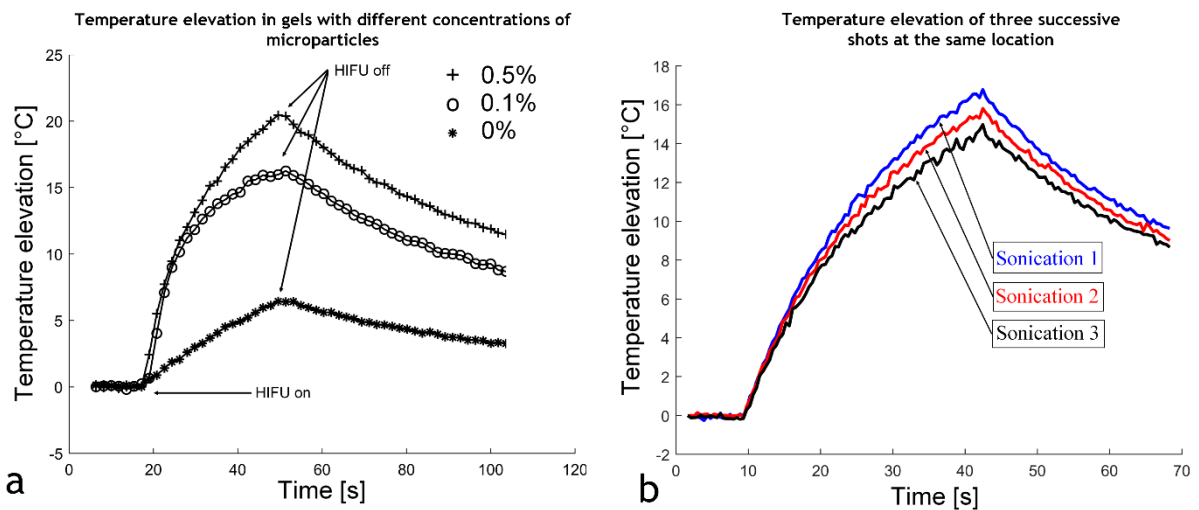
912



913

914

915 **Figure 4.** 19F MRI image of sliced gel with different MSD concentration, from left to right : 2%, 0.5%, 1%, 0.1%
916 and without MSD (overlaid frame in the zero-signal area).
917



918

919

920

921

922 **Figure 5.** a) Evolution of temperature at the centre of the sonication trajectory in absorbent gels at different
923 MSD concentration (see legend) during HIFU exposure. b) Impact of HIFU repetitions on temperature rising
924 (non-absorbent gel). The same acoustic parameters were applied after 5 minutes delay at the same location.
925 The ulterior sonications gradually induce less thermal effect. The blue line corresponds to the first sonication,
926 the red line corresponds to the second sonication and the black line to the third sonication.
927
928